Dynamics of a droplet on a polymer brush in channel flow

Fong Yew Leong[a)] and Duc-Vinh Le

A*STAR Institute of High Performance Computing, 1 Fusionopolis Way, Connexis, Singapore 138632.

ABSTRACT

Using Dissipative Particle Dynamics, we simulate an immiscible oil droplet on a polymer brush under a channel flow. Above a critical flow velocity, the droplet slides on the brush surface with contact angle hysteresis. Interestingly, we found the critical sliding velocity to be constant across droplet sizes and interphase interactions. Further increase in flow velocity results in droplet detachment and lift-off from the brush surface. Under poor solvent conditions, large droplets may deform into an airfoil shape, increasing the critical lift-off velocity. On an oleophilic brush, the droplet desorbs and spreads, instead of lift-off. Together, our results show surprisingly rich dynamics coupling three-way interactions between either soft or liquid phases. The present study has implications on the design of polymer brushes as well as the removal of droplets from soft surfaces using hydrodynamics.

[a)] Author to whom correspondence should be addressed. Electronic mail: leongfy@ihpc.a-star.edu.sg

I. INTRODUCTION

Removal of particles from surfaces has important applications in many industrial processes, such as contamination control in lithography processing[1], graphene production[2] and marine biofouling[3]. Under hydrodynamics shear, a particle may remain at rest,[4] slide,[5] rotate[6] or lift-off from the surface.[7] The near-wall mobility of the particle depends on a balance of forces, including gravitational, hydrodynamic drag, lift and electrostatic forces,[4,8,9] and this has been a subject of academic interest since the seminal works of Goldman et al.[10] and Saffman[11].

In more recent years, research interests have shifted to more deformable particles, or liquid droplets, on functionalized soft substrates.[12–16] Notably, polymers can be grafted at high densities on a surface to form so-called polymer brushes,[17] which have found applications in smart adhesives,[18] sensors,[19] switches,[20] thermoregulation,[21] antibiofouling,[22] lubrication[23] and anti-fog coatings.[24] Since the polymers are tethered on one end, the brush surface is constrained translationally such that a droplet experiences different wetting behavior compared to that of rigid substrates.[25,26] In particular, the contact angle of a droplet-brush system was found to increase with increasing softness of the brush, unlike other soft elastomeric substrates.[27]

When a droplet is dragged on the surface of a polymer brush, lubrication forces between droplet and brush leads to friction reduction[28] and possibly lift-off.[29] In a polymer-brushed nanochannel, the transport of a nanodroplet has been shown to depend on the friction properties of the brush, which is governed by the bending stiffness of the constituent polymers.[30] More recently it was found that the addition of grafted nanoparticles in the form of nanobearings does not significantly decrease lubrication between polymer-brushed surfaces.[23] However, these studies assume forced translocation and do not address the perhaps more practical problem of hydrodynamic removal of droplets or particles from polymer brushes. Elsewhere, it has been

reported that strong hydrodynamic shear on a pristine polymer brush leads to wave-like undulations or even flow inversion.[31] This has implications on biological flows over endothelial glycocalyx, a macromolecular layer lining the inner walls of vessels *in vivo*, that affects vascular permeability and regulates clotting and immune response.[32] The presence of the glycocalyx has significant effects on the flow dynamics of red blood cells in microcapillaries.[33]

At present, it is not clear how droplets would behave under similar flow conditions on soft substrates, and what drag and lift forces are required for detachment.[7] Theoretical studies exist for sliding,[34] rolling[35] and lifting[36] of macroscopic droplets driven by gravity on an inclined slope,[14] but they do not adequately explain the behavior of microscale droplets on soft substrates, such as polymer brushes. Simulations of droplets on polymer brushes are limited to rigid particle behavior[23] without significant deformation and solvent contribution.[29] Elsewhere, studies of droplet behavior on fibrous porous media are of relevance due to physical similarities in geometric structures, surface topography and potential imbibition.[37–39]

In this study, we use the dissipative particle dynamics (DPD) method[40] to study the behavior of an immiscible droplet on polymer brush under hydrodynamic shear. Our model presents a unique coupled three phase problem, where all three phases are not only immiscible but fluid-like and soft, leading to interactive dynamics of droplets under stress.

II. METHODS

A. Model

The dissipative particle dynamics (DPD) method, first conceived by Hoogerbrugge and Koelman[40] and later formalized by Groot, Español and Warren,[41,42] is a mesoscale technique that

uses soft conservative interactions to achieve effective coarse-graining, obeys fluctuation-dissipation theorem and exhibits hydrodynamic behavior at long time scales. DPD has been employed to study the dynamics of polymer brushes between walls,[43] under shear[44] and compression.[45]

DPD particles represent clusters of atoms or molecules. Each particle evolves in time according to Newton's equations of motion,

$$m_i \dot{\boldsymbol{v}}_{\boldsymbol{i}} = \sum_{i \neq j} \left(\boldsymbol{F}_{ij}^{C} + \boldsymbol{F}_{ij}^{D} + \boldsymbol{F}_{ij}^{R} \right), \tag{1}$$

where m_i and $\boldsymbol{v}_{\boldsymbol{i}}$ are the mass and velocity of particle i.

The conservative force $\boldsymbol{F}_{\boldsymbol{ij}}^{\boldsymbol{C}}$ acting between particle i and j separated by a distance $r_{ij} = \left| \boldsymbol{r}_{\boldsymbol{i}} - \boldsymbol{r}_{\boldsymbol{j}} \right|$ is

$$\boldsymbol{F}_{\boldsymbol{ij}}^{\boldsymbol{C}} = \begin{cases} a_{ij} \left(1 - \frac{r_{ij}}{r_c} \right) \hat{\boldsymbol{r}}_{\boldsymbol{ij}} & r_{ij} < r_c \\ 0 & r_{ij} \geq r_c \end{cases}, \tag{2}$$

where a_{ij} is the repulsion parameter and $\hat{\boldsymbol{r}}_{\boldsymbol{ij}} = \boldsymbol{r}_{\boldsymbol{ij}} / r_{ij}$ is the distance unit vector between particle i and j. The repulsion force is linear up to a cutoff radius r_c, which sets the characteristic length scale of the DPD simulation.

The dissipative force $\boldsymbol{F}_{\boldsymbol{ij}}^{\boldsymbol{D}}$ depends on the relative momentum $\boldsymbol{v}_{\boldsymbol{ij}} = \boldsymbol{v}_{\boldsymbol{i}} - \boldsymbol{v}_{\boldsymbol{j}}$, as

$$\boldsymbol{F}_{\boldsymbol{ij}}^{\boldsymbol{D}} = -\gamma_{ij} \omega^{D}(r_{ij}) (\boldsymbol{r}_{\boldsymbol{ij}} \cdot \boldsymbol{v}_{\boldsymbol{ij}}) \hat{\boldsymbol{r}}_{\boldsymbol{ij}}, \tag{3}$$

where γ_{ij} is the friction coefficient and the dissipative weight function $\omega^{D}(r_{ij})$ is

$$\omega^{D}(r_{ij}) = \begin{cases} \left(1 - \frac{r_{ij}}{r_c} \right)^2 & r_{ij} < r_c \\ 0 & r_{ij} \geq r_c \end{cases}. \tag{4}$$

The random force $\boldsymbol{F}_{ij}^{R}$ is

$$\boldsymbol{F_{ij}^{R}} = \sigma_{ij}\omega^{R}(r_{ij})\frac{\zeta_{ij}}{\sqrt{\Delta t}}\hat{\boldsymbol{r}}_{\boldsymbol{ij}}, \tag{5}$$

where σ_{ij} is the noise amplitude, ζ_{ij} is a pseudo-random variable sampled from a Gaussian distribution with zero mean and unit variance. These equations obey the fluctuation-dissipation theorem, which reads,

$$\gamma_{ij} = \frac{\sigma_{ij}}{2k_BT} \quad \text{and} \quad \omega^{D}(r_{ij}) = \left[\omega^{R}(r_{ij})\right]^2, \tag{6}$$

where $\omega^{R}(r_{ij})$ is the weight function for the random force. Here, we set $\gamma_{ij} = 4.5$ and $\sigma_{ij} = 3$ following earlier studies.[41]

The polymer chains in the brush are modelled using finite extensible nonlinear elastic potential (FENE)[46]

$$\boldsymbol{F_{ij}^{P}} = -2kr_{max}^2\left[\frac{r_{ij}-r_{eq}}{R^2-(r_{ij}-r_{eq})^2}\right]\hat{\boldsymbol{r}}_{\boldsymbol{ij}} \qquad r_{ij} - r_{eq} < r_{max}, \tag{7}$$

where k is the spring constant, r_{eq} is the equilibrium distance between adjacent monomers and r_{max} is the maximum extensibility. The rigidity of each polymer chain is modelled by harmonic bending potential as

$$U_b(\theta) = \frac{k_b}{2}\theta^{\mathbf{2}}, \tag{8}$$

where k_b is the bending stiffness and θ is the angle between two consecutive segments along the polymer described by

$$\cos\theta = \frac{(\boldsymbol{r_{i-}})(\boldsymbol{r_{i+}})}{|\boldsymbol{r_{i-}}||\boldsymbol{r_{i+}}|}, \tag{9}$$

where $\boldsymbol{r_{i-}} \equiv \boldsymbol{r_i} - \boldsymbol{r_{i-1}}$ and $\boldsymbol{r_{i+}} \equiv \boldsymbol{r_{i+1}} - \boldsymbol{r_i}$.

B. Setup

We simulate channel flow in a box of dimensions $\{L_x, L_y, L_z\} = \{100, 100, 10\}$, with periodic boundary conditions imposed on the x- and z- boundaries (**Fig. 1a**). In this study, we refer to three types of particles corresponding to the immiscible phases of interest, specifically solvent (S), oil (O) and polymer (P), with intra- and inter-phase interactions as shown in **Fig. 1b**. Solvent particles are initialized at a number density $\rho_S = 3$, so that $n_S = 300{,}000$. No penetration condition is imposed on the vertical boundaries using specular reflection condition so that $v_y \rightarrow -v_y$ at $y = \{0, L_y\}$. Surface density is matched using parallel frozen walls formed by solvent particles 2 units deep at density $\rho_{wall} = 3$. On the bottom wall, 1000 polymers are grafted at 40 monomers per polymer chain at regular intervals, with a grafting density $\sigma_{graft} \equiv n_P/(L_x L_z) = 1$, where n_P is the number of grafted polymers.

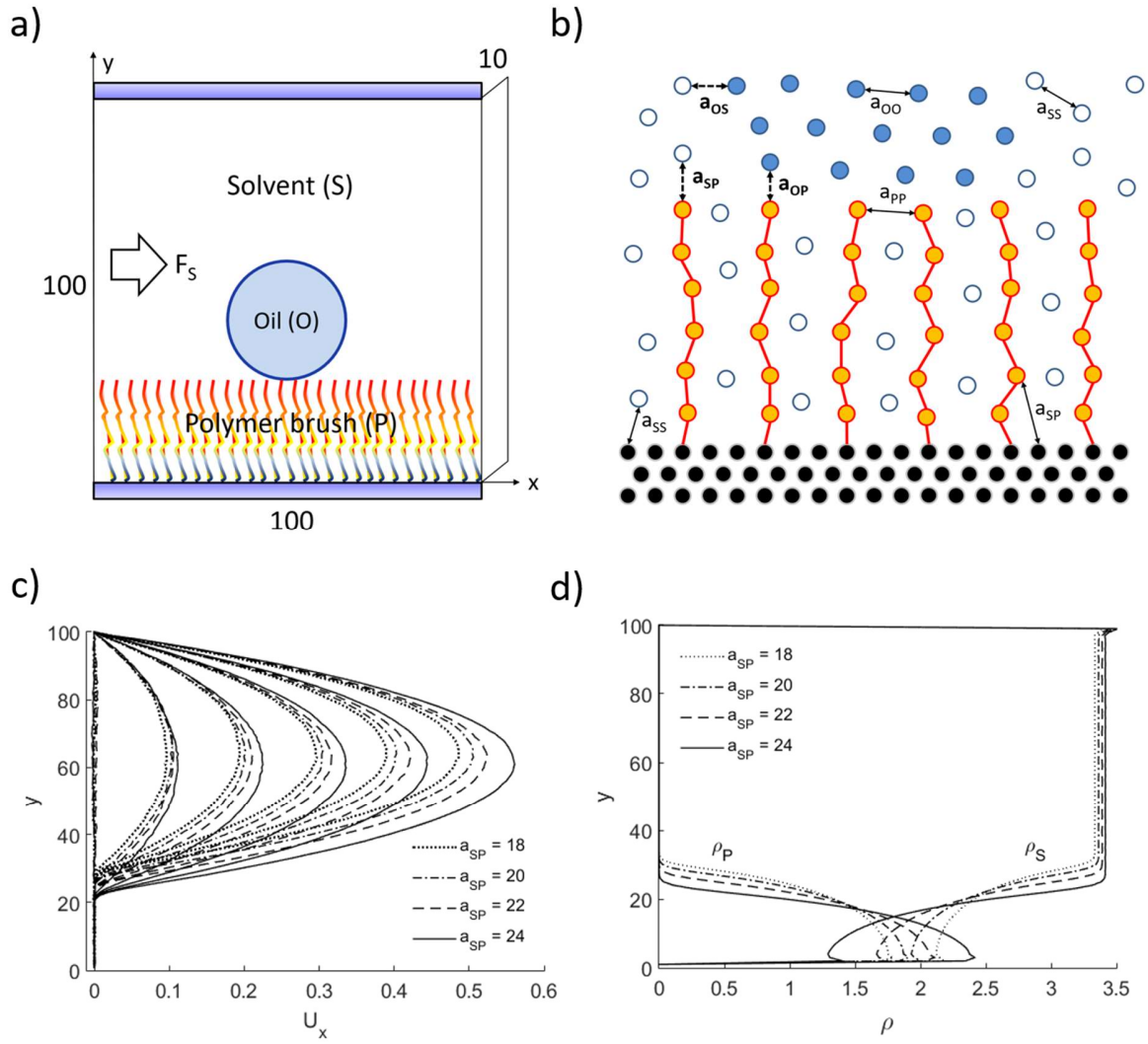

Fig. 1. (a) Schematic diagram of DPD model setup for channel flow of solvent (S) over an oil (O) droplet on a polymer brush (P). Cartesian box dimensions are $\{L_x, L_y, L_z\} = \{100, 100, 10\}$, with periodic boundary conditions imposed on the x- and z- boundaries. (b) Interactions between DPD particles of same and different (dashed arrow) phases. Wall particles are frozen solvent particles. (c) Time-averaged velocity profiles U_x in a horizontal channel driven by solvent force F_x in increments of 5×10^{-5} depend on solvent-brush repulsion a_{SP}. (d) Time-averaged density profiles of the solvent ρ_S and polymer ρ_P phases, with original solvent density $\rho_S = 3$.

C. Physical units

The reference DPD units are $r_c = 1$, $m_i = 1$, $k_BT = 1$ for length, mass and energy respectively. The density of the solvent particles is $\rho_S = 3$, which means for water under room temperature, the solvent-solvent repulsion is $a_{SS} = 25$.[31] Other intra-phase repulsions are assumed to be similarly scaled, i.e. $a_{OO} = a_{PP} = 25$. As for inter-phase repulsions, the oil-polymer repulsion is also defaulted as $a_{OP} = 25^*$, so the interface is interaction-neutral, the solvent-polymer repulsion parameter is set at a lower value of $a_{SP} = 20^*$ which yields good solvent conditions, and the oil-solvent repulsion parameter is set at $a_{OS} = 70^*$ which yields good immiscibility using Irving-Kirkwood method.[47] For clarity, the superscript asterisks refer to base case values for inter-phase repulsions.

The physical units depend on the degree of coarse-graining required for the simulation, in which case following the normalized spacing between glycocalyx filaments, the physical length scale is taken as $l_{phys} = 24\ nm$.[31] Based on the density of water $\rho = 1000\ kg/m^3$ and viscosity of water $\eta = 10^{-3}\ Pa \cdot s$ at $T = 300\ K$, we find the physical mass scale $m_{phys} \equiv \rho {l_{phys}}^3 = 1.38 \times 10^{-20}\ kg$, energy scale $e_{phys} \equiv k_BT = 4.14 \times 10^{-21}\ J$, and time scale $t_{phys} \equiv \eta {l_{phys}}^3 / e_{phys} = 3.34\ \mu s$.

For the FENE potential, the parameters in DPD units are $k = 25$, $k_b = 0$, $r_{eq} = 0.86$ and $r_{max} = 1$.[31]

D. Implementation

The DPD simulations are implemented using NVT ensemble in the DL_MESO DPD package.[48] The initial solvent-polymer system is first equilibriated for one million time steps at time intervals of $\Delta t = 0.01$, before running the actual simulation for another million time steps with channel flow. To generate pressure-driven flow in the channel, we apply an additional constant horizontal body force to each solvent particle $\boldsymbol{F_S} = \{F_x, 0, 0\}$ before the velocity update step. This allows the solvent phase to exchange momentum with otherwise passive polymer phases.

For a solvent-polymer system (without oil), **Fig. 1c** shows that the solvent velocity profiles driven by F_x in increments of 5×10^{-5} depend on solvent-polymer repulsion a_{SP}, a parameter which sets the height of the polymer brush as shown by polymer density ρ_P profiles (**Fig. 1d**). At $F_x = 10^{-3}$, the Reynolds number of the channel is $Re{\sim}0.0138$. Under good solvent conditions ($a_{SP} = 20$), polymers are solvated and extended, which dissipates the pressure gradient. Solvent velocities in the channel are reduced, despite the smaller gap between the brush surface and the top of the channel. In each case, the maximum channel velocity U_{max} is proportional to the applied driving force F_x and the solvent velocity U^* is the solvent velocity evaluated at the position of droplet center. Mean polymer brush heights are $h_{brush} \cong \{30, 28, 25\}$ for $a_{SP} = \{20,22,24\}$.

The oil droplet consists of oil particles initialized from solvent particles found within a virtual circular cylinder of radius R and depth L_z, centered and adjusted so that the oil droplet is resting on the polymer brush surface without buoyancy effects. In this study, four droplet radii are considered, namely $R = \{10, 15, 20, 25\}$, which consist of $N_O = \{9723, 21093, 39028, 61163\}$ oil particles respectively.

III. RESULTS

A. Solvent-polymer repulsion

The solvent condition[49] of a polymer brush depends on the solvent-polymer repulsion a_{SP}. For an oil droplet on a polymer brush, an increase in a_{SP} could lead to the droplet flattening and sinking into the brush layer, as shown in **Fig. 2a** for a droplet of initial radius $R = 10$. With an increase in a_{SP} from 20 (good solvent condition) to 24 (poor solvent condition), the droplet flattens so that its height decreases from 19.7 to 17.7 and sinks so that its absorption depth (sub-surface) increases from 3.8 to 8.6. In contrast, for a larger droplet of $R = 20$, the droplet height decreases from 38.3 to 33.7 but the absorption depth increases from 3.8 to 5.6 only. The bulk of the droplet remains above the surface of the polymer brush.

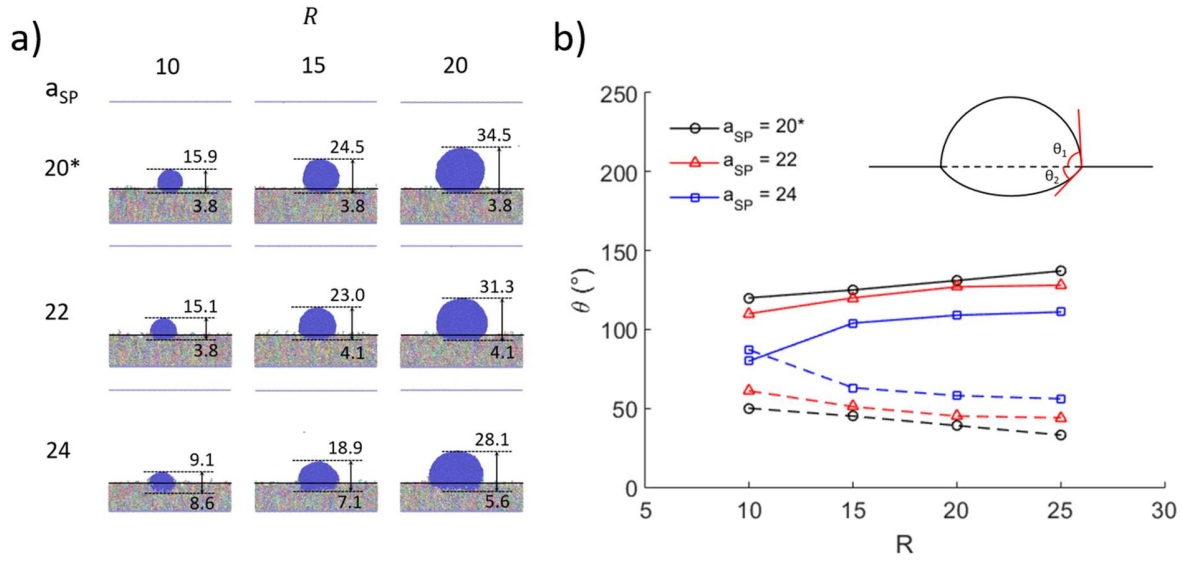

Fig. 2. (a) Increasing solvent-polymer repulsion a_{SP} causes an oil droplet of radius R to flatten and sink into polymer brush ($t = 10^4$). Other interaction parameters are $a_{OP} = 25^*$ and $a_{OS} = 70^*$. (b) Equilibrium contact angles above (θ_1; continuous) and below (θ_2; dashed) brush surface depend on R for various a_{SP}.

A stationary oil droplet on a polymer brush manifests static contact angles at the three-phase contact line due to competitive interfacial tensions. The balance results in either Young's law for hard substrates, or Neumann triangle for soft substrates,[50] including gels and polymer brushes. Following Cao and Dobrynin,[51] we refer to the Neumann contact angles as the angle formed by the drop above and below the brush surface (denoted as θ_1 and θ_2 respectively). As shown in **Fig. 2b**, both θ_1 and θ_2 vary depending on droplet radius for various a_{SP}. Note that the sums of angles $\theta = \theta_1 + \theta_2$ are similar for each case, and there is a reversion in angles $\theta_1 < \theta_2$ for the case of $R = 10$ and $a_{SP} = 24$.

For a channel flow driven by solvent driving force ($F_x > 0$), an oil droplet may deform and slide on the surface of the polymer brush (**Fig. 3a**). Contact angle hysteresis is observed, where the advancing angle (in blue) is different from the receding angle (in red). With increase in driving force F_x, the advancing upper angle $\theta_{1,a}$ increases, the advancing lower angle $\theta_{2,a}$ decreases while both the receding angles θ_r remains relatively constant. The latter observation underlies strong pinning effect along the receding edge, as the droplet is visibly inclined in the flow direction. With increasing solvent-polymer repulsion a_{SP}, the advancing upper angle $\theta_{1,a}$ decreases, the advancing lower angle $\theta_{2,a}$ increases, while receding upper angles $\theta_{1,r}$ decreases.

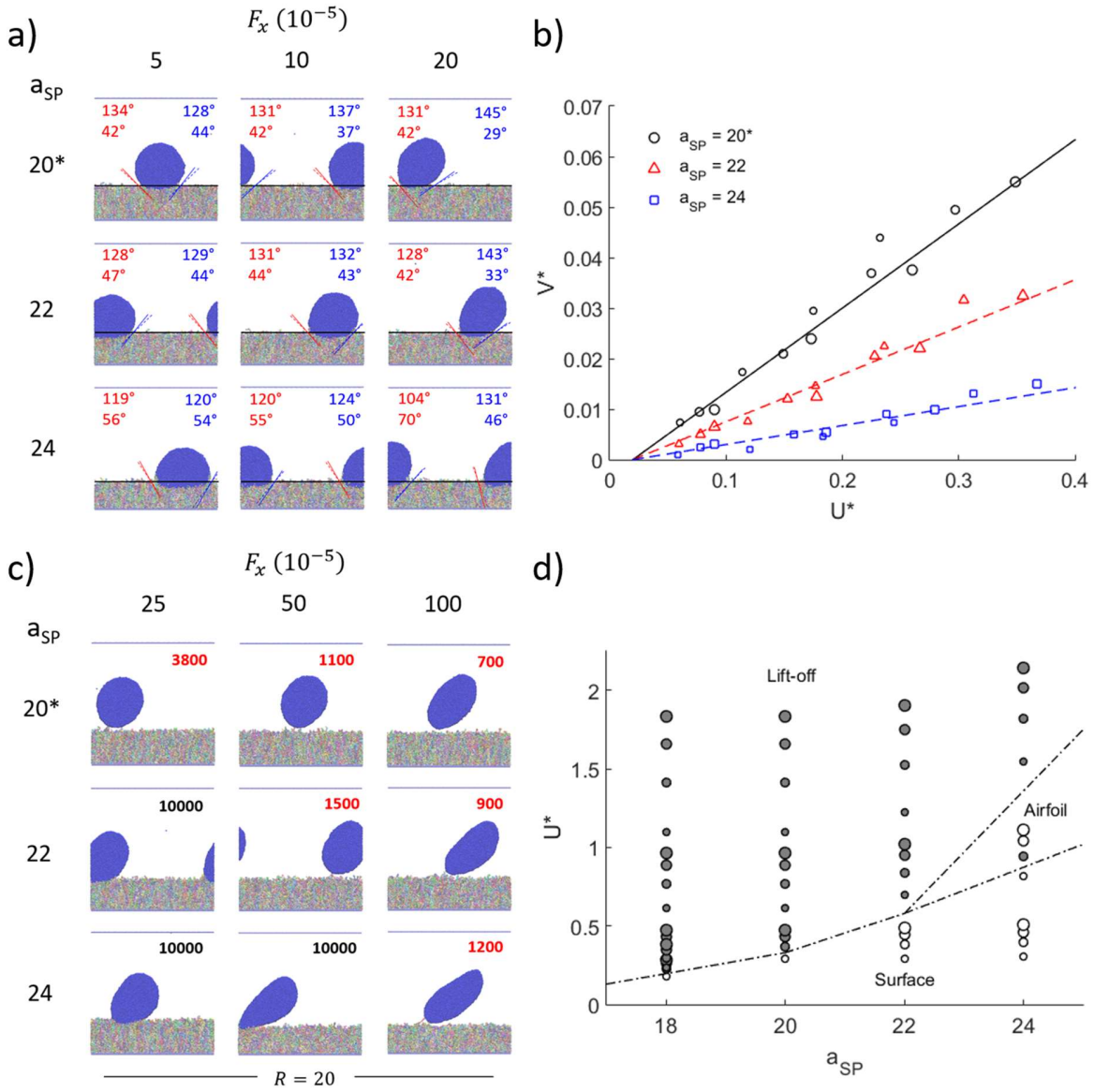

Fig. 3. (a) Snapshots of a droplet $R = 20$ sliding on polymer brush surface driven by channel flow varying solvent-polymer repulsion a_{SP} ($a_{OP} = 25^*$, $a_{OS} = 70^*$) with contact angle hysteresis ($t = 10^4$). Panels show upper (θ_1) and lower (θ_2), receding (θ_r, left) and advancing (θ_a, right) contact angles. (b) Time-averaged velocity of oil droplet V^* on polymer brush driven by flow velocity U^* evaluated at droplet center for various a_{SP}. Relative symbol sizes denote droplet sizes $R = \{10, 15, 20, 25\}$. Intercept shows the critical velocity for droplet sliding

U_{cs}^{*}~0.02. (c) Snapshots for droplet during lift-off at indicated times (red), and for droplets which fail to lift-off at simulation end time $t = 10^4$ (black). (d) Phase diagram of flow velocity U^* leading to droplet lift-off (filled symbols) depending on solvent-polymer repulsion a_{SP}. Relative symbol sizes denote droplet sizes $R = \{10, 15, 20, 25\}$. Within the airfoil regime, larger droplets may deform into an airfoil shape sliding under shear.

For a droplet on hard substrate, the drag force is approximated by the equivalent drag force on a rigid sphere of the same apparent diameter.[52] To see how droplets slide on soft polymer brush, **Fig. 3b** shows a plot of the time-averaged surface velocity V^* of an oil droplet on polymer brush against the channel flow velocity U^* evaluated at a vertical position of one radius R above the brush surface (see **Fig. 1c**). Under poor solvent conditions ($a_{SP} = 24$), we see that the droplet velocity scales linearly with solvent flow velocity V^*~U^* without significant droplet size dependence. In contrast, under good solvent conditions ($a_{SP} = 20$), the data is comparatively more scattered with droplet size dependence, where larger droplets slide at a low velocity compared to smaller ones for the same flow velocity. By inspection, the droplet velocity trend lines converge at a common intercept so the apparent critical velocity before a droplet starts to slide is U_{cs}^{*}~0.02.

Under strong channel flows ($F_x > 20 \times 10^{-5}$), an oil droplet may detach and lift-off from the brush surface (**Fig. 3c**), if the hydrodynamic lift force is strong enough to overcome the adhesion force holding the droplet to the brush (see Supporting Information). The solvent driving force F_x necessary for droplet lift-off increases with solvent-polymer repulsion a_{SP}. At $a_{SP} = 24$, the droplet at the point of detachment is elongated at an inclined axis. This is reminiscent of the classic solution of an ellipsoidal droplet in linear shear flow,[53] whose deformation depends on its

capillary number $Ca = \eta\dot{\gamma}R/\sigma$, where η is the solvent viscosity, $\dot{\gamma}$ is the flow shear rate and σ is the interfacial tension between oil and solvent phases. Incidentally, the observed droplet shapes during sliding and lift-off are also in qualitative agreement with those of vesicles under strong shear.[54]

Soft lubrication refers to lift force produced as an object translates in a linear shear flow near a soft substrate.[55–57] Inspection of **Fig. 3c** shows an asymmetric deformation of the brush surface below the droplet, which suggests that lubrication force applies similarly, despite physical differences between droplets and rigid bodies.

Fig. 3d shows the phase diagram for droplet lift-off depending on flow velocity U^* and solvent-polymer repulsion a_{SP}. The critical flow velocity required for lift-off U_{cl}^* (dashed lines) increases with a_{SP}. For $a_{SP} = 24$ (poor solvent), larger droplets deform into an airfoil shape (see **Fig. 3c**; center bottom) under shear, which reduces the lift force experienced by the droplet. This is reflected as an increase in the critical lift-off velocity U_{cl}^* as indicated on the phase diagram ('airfoil' regime).

B. Oil-polymer repulsion

The miscibility of oil in polymer brush depends on the interfacial repulsion between the two phases. For low oil-polymer repulsion $a_{OP} = 20$ (oleophilic) equal or less than the solvent-polymer repulsion $a_{SP} = 20^*$, an oil droplet could be absorbed into the brush (**Fig. 4a**). For a polymer brush of thickness $h_{brus} = 30$, we find that a droplet of radius $R = 10$ is fully submerged, whereas a larger droplet of $R = 20$ is only partially submerged. It follows that the extent of submergence depends on thickness ratio $2R \sim h_{brush}$. For stronger oil-polymer

repulsion a_{OP}, the absorption depth is relatively insensitive to droplet sizes (5.3 – 6.5), with only marginal decrease seen for larger droplets. **Fig. 4b** shows that both θ_1 and θ_2 depends on droplet radius for various a_{OP}. For $a_{OP} = 20$, the angle ratio is less than one ($\theta_1/\theta_2 < 1$) when $R < 25$. For $a_{OP} > 20$, both θ_1 and θ_2 are independent of a_{OP}.

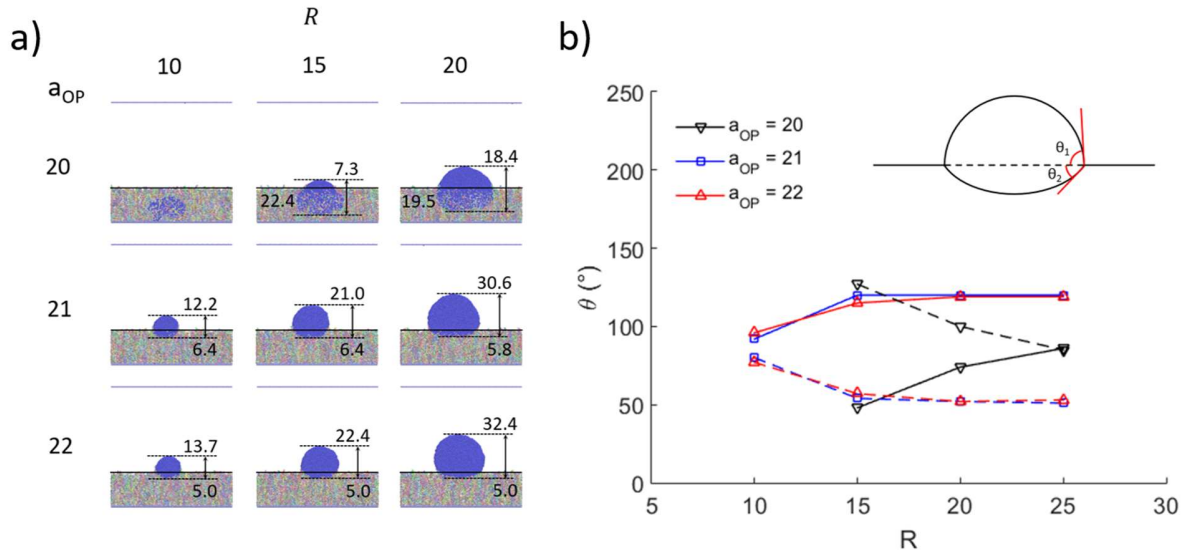

Fig. 4. (a) Low oil-polymer repulsion a_{OP} can cause an oil droplet of radius R to be fully or partially absorbed into polymer brush ($t = 10^4$). Other interaction parameters are $a_{SP} = 20^*$ and $a_{OS} = 70^*$. (b) Equilibrium contact angles above (θ_1; continuous) and below (θ_2; dashed) brush surface depend on the droplet radius R for various a_{OP}.

For a channel flow driven by solvent driving force, an oil droplet may deform and slide even if it is partially submerged (**Fig. 5a**). Contact angle hysteresis is observed, where the advancing angle (in blue) is different from the receding angle (in red). Both advancing and receding θ_1 angles increase with oil-polymer repulsion a_{OP}. With increase in driving force F_x, the advancing

upper angle $\theta_{1,a}$ increases, the advancing lower angle $\theta_{2,a}$ decreases and the receding $\theta_{1,r}$ angle decreases slightly. As before, the droplet is tilted in the flow direction as it slides on the brush surface, including any submerged volume ($a_{OP} = 20$). With increasing oil-polymer repulsion a_{OP}, the advancing upper angle $\theta_{1,a}$ increases and the advancing lower angle $\theta_{2,a}$ decreases, the receding upper angles $\theta_{1,r}$ increases and the receding upper angles $\theta_{2,r}$ decreases. Since a_{SP} and a_{OP} are competitive interactions, their effects on contact angles are expected to be reversed, and this is shown to be indeed the case. Separately, oil droplet absorption ratio within polymer brush depends on imposed flow rates and quality of submergence (see Supporting Information).

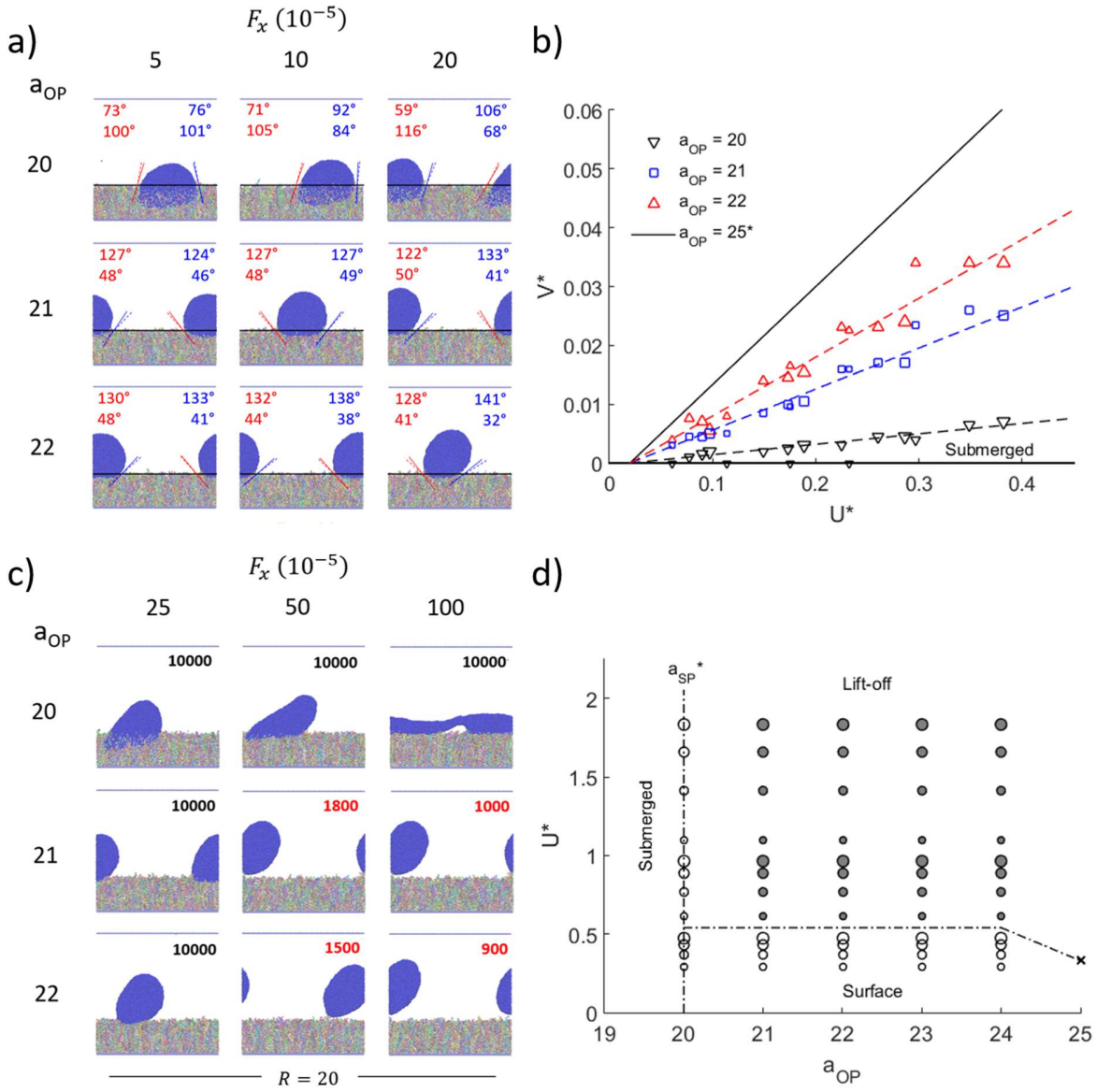

Fig. 5. (a) Snapshots of a droplet of radius R = 20 sliding on polymer brush surface driven by channel flow varying oil-polymer repulsion a_{OP} ($a_{SP} = 20^*$, $a_{OS} = 70^*$) with contact angle hysteresis ($t = 10^4$). Panels show upper (θ_1) and lower (θ_2), receding (left, red) and advancing (right, blue) contact angles. (b) Time-averaged velocity of oil droplet V^* on polymer brush driven by flow velocity U^* evaluated at droplet center for various a_{OP}. Relative symbol sizes denote droplet sizes $R = \{10, 15, 20, 25\}$. For $a_{OP} = 20$, the droplet could be partially ($2R \geq$

h_{bru}) or completely submerged ($2R < h_{brus}$) where $V^* = 0$**.** Black line refers to linear regression for the base case $a_{OP} = 25^*$. Intercept shows critical velocity for droplet sliding U_{cs}^*~0.02. (c) Snapshots for droplet during lift-off at indicated times (red), and for droplets which fail to lift-off at simulation end time $t = 10^4$ (black), for various oil-solvent repulsion a_{OP}. For $a_{OP} = 20$, the droplet may desorb and spread on the brush surface instead of lift-off. (d) Phase diagram shows that lift-off is only possible for surface droplets above the submergence criterion ($a_{OP} > a_{SP} = 20^*$). The critical lift-off velocity U_{cl}^* remains constant at ~0.53, up to $a_{OP} = 24$. For $a_{OP} = 25$, U_{cl}^* decreases to ~0.33 (indicated by cross symbol).

To see if linear velocity scaling apply to oleophilic brushes ($a_{OP} \leq 20$), we plot the time-averaged surface velocity V^* of an oil droplet driven by channel flow velocity U^* evaluated at droplet center (**Fig. 5b**). For $a_{OP} = 20$, the droplet could be either partially submerged ($2R \geq h_{brush}$), so that its velocity linearly varies with flow velocity, or it could be small enough to be completely submerged ($2R < h_{brush}$). It is interesting to note that the critical velocity for droplet sliding U_{cs}^* is, once again, well approximated by ~0.02 (see **Fig. 3b**) for all a_{OP} including $a_{OP} = 20$ where the droplet may be partially submerged.

As shown previously, an oil droplet may detach and lift-off from the brush surface under strong flows. However, for $a_{OP} = 20$, an increase in U^* only cause the partially submerged droplet to desorb and spread on brush surface, without lift-off (**Fig. 5c**). Phase diagram shows for $a_{OP} = 20$, droplet lift-off was not observed for any droplet size and solvent driving force (**Fig. 5d**). Instead, lift-off is only observed for surface droplets ($a_{OP} > 20$), where the critical lift-off

velocity U_{cl}^{*}~0.53 appears insensitive to a_{OP} until $a_{OP} = 24$. For base case $a_{OP} = 25^{*}$, the critical lift-off velocity decreases sharply to U_{cl}^{*}~0.33 (indicated by cross symbol).

C. Oil-solvent repulsion

The surface tension of the oil droplet depends on the oil-solvent repulsion a_{OS} (see Supporting Information). **Fig. 6a** shows that the droplets do not absorb into the brush significantly across a range of oil-solvent repulsions a_{OS}. Also, the apparent contact angles are relatively insensitive to the droplet radius R and oil-solvent repulsion a_{OS} (**Fig. 6b**).

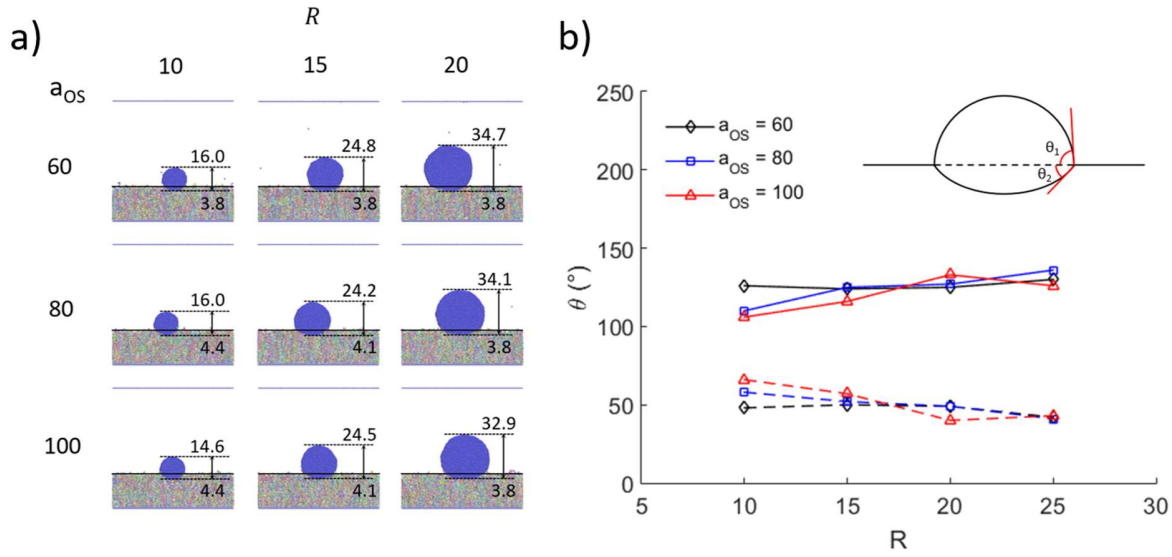

Fig. 6. (a) Oil-solvent repulsion a_{OS} has little effect on droplet morphology and brush absorption ($t = 10^4$). Other interaction parameters are $a_{SP} = 20^{*}$ and $a_{OP} = 25^{*}$. (b) Equilibrium contact angles above (θ_1; continuous) and below (θ_2; dashed) brush surface are relatively insensitive to the droplet radius R and oil-solvent repulsion a_{OS}.

One may therefore expect the flow-driven dynamics to be similar, but there are some differences (**Fig. 7a**). Contact angle hysteresis is observed for a droplet with low surface tension ($a_{OS} = 60$) but it diminishes with increasing a_{OS}; for $a_{OS} = 100$, the droplet slides on the surface as if it were a rigid spherical particle. As before, we plot the time-averaged surface velocity V^* of an oil droplet on polymer brush driven by channel flow velocity U^* evaluated at droplet center (**Fig. 7b**). For the same flow velocity U^*, a decrease in oil-solvent repulsion a_{OS} results in an increase in droplet velocity V^*. For $a_{OS} = 60$, we see that larger droplets can achieve lift-off at higher flow velocities (filled symbols).

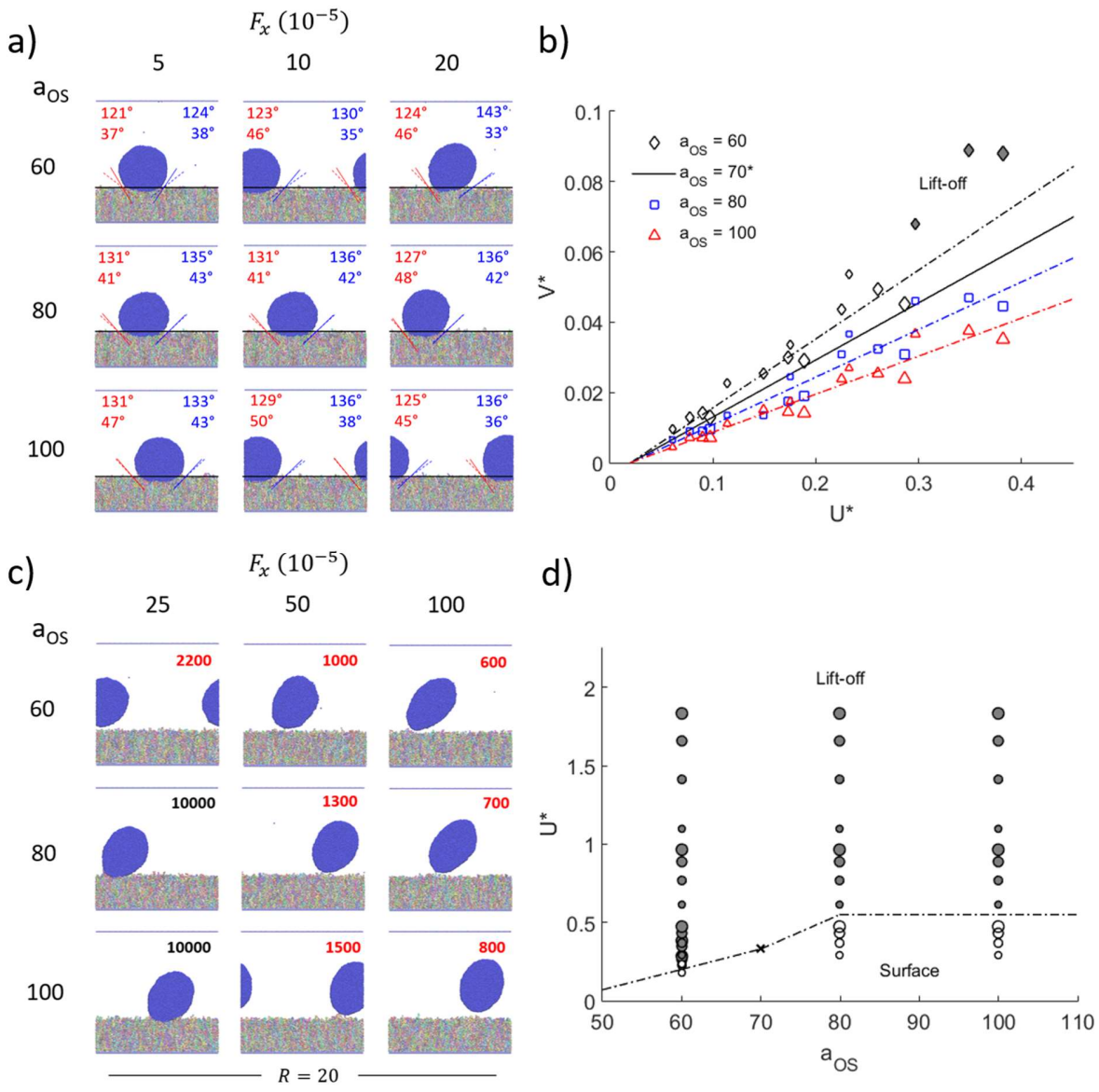

Fig. 7. (a) Driven by channel flow, a droplet of radius R = 20 slides on the polymer brush surface varying oil-solvent repulsion a_{OS} ($a_{SP} = 20^*$ and $a_{OP} = 25^*$) showing deformation and contact angle hysteresis ($t = 10^4$). Panels show upper (θ_1) and lower (θ_2), receding (left, red) and advancing (right, blue) contact angles. (b) Effect of a_{OS} on time-averaged droplet velocity V^* on polymer brush driven by solvent flow velocity U^* evaluated at droplet center. Relative symbol sizes denote droplet sizes $R = \{10, 15, 20, 25\}$. Large droplets with low a_{OS} may lift-off

(filled symbols). (c) Snapshots of droplets during lift-off at indicated times (red), and droplets which fail to lift-off at simulation end time $t = 10^4$ (black), for various oil-solvent repulsion a_{OS}. (d) Phase diagram shows for $a_{OS} \geq 80$, the critical lift-off velocity U_{cl}^*~0.53 is insensitive to a_{OS}. U_{cl}^* reduces to ~0.33 (cross symbol) for $a_{OS} = 70$ and ~0.20 for $a_{OS} = 60$.

As with previous cases, an oil droplet may detach and lift-off from the brush surface under strong flows (**Fig. 7c**). Nevertheless, the effect of a_{OS} (surface tension) is shown here to reduce deformation of the droplet from ellipse to circular, and interestingly, align the droplet along the vertical axis at the time of detachment. Phase diagram shows for $a_{OS} \geq 80$, the critical lift-off velocity U_{cl}^*~0.53 appears insensitive to a_{OS} (**Fig. 7d**). For base case $a_{OS} = 70$, U_{cl}^* reduces to 0.33 and for $a_{OS} = 60$, U_{cl}^* further reduces to 0.20. Below $a_{OS} = 60$, the oil phase is increasingly miscible with solvent phase (not shown).

D. Polymer rigidity

In this section, we explore the effects of polymer brush rigidity[30] on both static and dynamic surface droplet behavior under base case conditions. Overall, an increase in brush rigidity promotes droplet desorption (**Fig. 8a**). In addition, we find that brush chain stiffness k leads to reduction in brush thickness but the bending stiffness k_b leads to stretched bonds and brush extension. Interestingly, the solvent flow above the brush increases with k and decreases with k_b (**Fig. 8b**). This is because the increased dissipation due to brush rigidity more than offset the effects due to reduction in channel width. The confluence of these factors, i.e. desorption and drag, means that droplet velocity slides faster in either case with brush rigidity playing a

dominant role (**Fig. 8c**). At higher flow rates, the droplet undergoes lift-off as before with an added observation that despite faster droplet velocities, stronger solvent force is now necessary for lift-off due to flow reduction by rigid brushes (**Fig. 8d**).

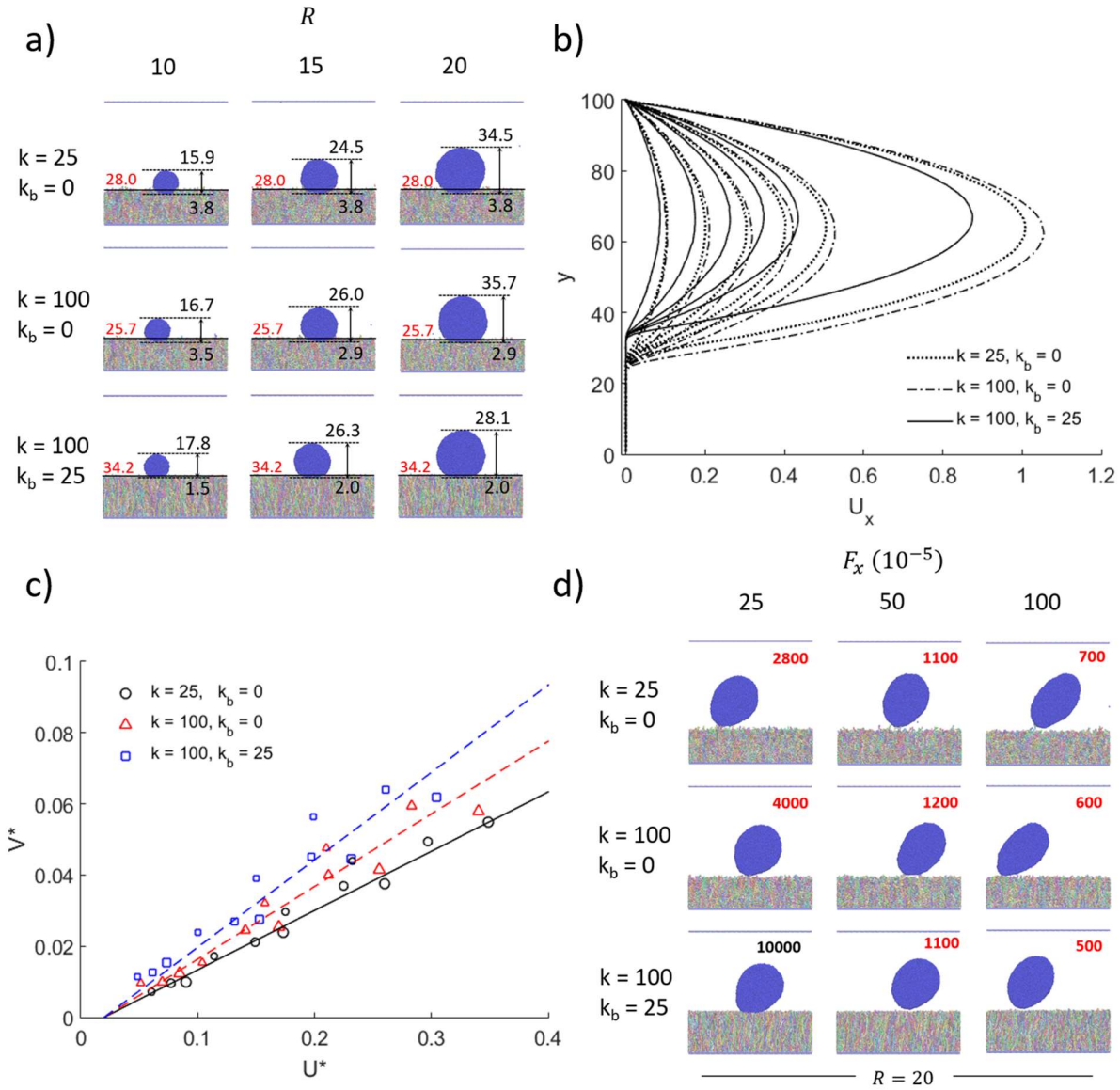

Fig. 8. Effects of increasing polymer chain stiffness k to 100 and bending rigidity k_b to 25 on droplet behavior under base conditions ($a_{SP} = 20^*$, $a_{OP} = 25^*$, $a_{OS} = 70^*$). (a) Both k and k_b promote droplet desorption. Polymer brush thickness (red) decreases with k and increases with

k_b. (b) Time-averaged velocity profiles U_x driven by solvent force F_x in increments of 5×10^{-5}. (c) Time-averaged droplet velocity V^* on polymer brush driven by solvent flow velocity U^* evaluated at droplet center. Relative symbol sizes denote droplet sizes $R = \{10, 15, 20, 25\}$. Intercept shows critical velocity for droplet sliding $U_{cs}^* \sim 0.02$. (d) Snapshots of droplets during lift-off at indicated times (red), and droplets which fail to lift-off at simulation end time $t = 10^4$ (black).

In addition, we note the relevance of our results in the flow of red blood cell in micro-capillaries with polymer brush walls, due to the competitive effects of the solvent flow reduction in channel and the relative increase in droplet sliding speed. Despite physical differences between vesicles and drops, this could help explain the non-linear dependence of red blood cell velocity on brush thickness.[33]

IV. DISCUSSION

Using Dissipative Particle Dynamics (DPD) simulations of three interacting immiscible phases (oil, solvent and polymer brush), we characterize both static and dynamic behavior of oil droplets on a polymer brush under a channel flow. Above a critical flow velocity, an oil droplet can be made to slide on the polymer brush. Interestingly, the critical sliding velocity was found to be constant (~ 0.02 in DPD units) across various droplet sizes and interphase interactions evaluated in this study. This is perhaps because the polymer brush, highly valued for its lubricating properties,[28] does not offer significant static resistance to motion; a stiffer interacting brush may be required to pin a droplet in place under low shear conditions.[30] In addition, our results show

that an oil droplet tends to slide faster under conditions of (1) low solvent-polymer repulsion, (2) high oil-polymer repulsion, (3) low oil-solvent repulsion and (4) rigid polymer brushes. Qualitatively, this suggests that droplet sliding can be promoted using a rigid polymer brush that is oil-repelling, has good solvent quality and surfactants which reduce the surface tension of the oil droplet in the solvent.

The degree of droplet absorption depends on its interaction with the polymer brush, so although the Young to Neumann transition cannot be universal,[27] the static behavior of droplet on polymer brush can be manipulated with the inclusion of solvent interactions with various absorption effects. As droplet slide on the brush driven by flow, we observed contact angle hysteresis in all cases, including droplets that ascribe to Neumann's law. We also found that the advancing angles are more sensitive to flow velocity than the receding angles, due to pinning at the receding edge as droplets deform and incline in the direction of the flow.

With increasing flow, a droplet could detach and lift-off from the brush surface into the solvent stream once the lift force overcomes the adhesion force. Under poor solvent conditions, stronger flows are required to remove an oil droplet as reflected by an increase in critical lift-off velocity. In this case, a sufficiently large droplet could deform into an airfoil shape which further increases the critical lift-off velocity.

For a strictly oleophilic brush, an oil droplet can be fully submerged if its size is smaller than the brush thickness; this has the effect of insulating the droplet from hydrodynamic forces above the brush surface, preventing lift-off. If the droplet is partially submerged, the exposed section is subjected to hydrodynamic forces so that the droplet can slide on the brush. With increasing flow, the droplet desorbs from the brush and spreads on its surface, but without detachment or lift-off. In this study, lift-off was not observed across all droplet sizes and channel flow

velocities. With a less oleophilic brush, there is a sharp transition whereby lift-off becomes possible under strong flows.

Finally, surface tension promotes droplet lift-off at low values but is moderated at higher values. Taken together, our results show a surprisingly rich outcomes in terms of three-way interactions between either soft or liquid phases, leading to sliding or lift-off depending on the strength of the imposed flow. The present study has implications on the design of polymer brushes as well as the propulsion or removal of small immiscible droplets from soft surfaces through hydrodynamic means.

SUPPLEMENTARY MATERIAL

See supplementary material for further discussion on lift forces, interfacial tension and dynamic absorption ratio.

CONFLICTS OF INTEREST

There are no conflicts to declare.

DATA AVAILABILITY STATEMENT

The data that support the findings of this study are available from the corresponding author upon reasonable request.

ACKNOWLEDGMENT

The computational work for this article was (fully/partially) performed on resources of the National Supercomputing Centre, Singapore (https://www.nscc.sg). This research was supported by A*STAR under the Pharos "Advanced Surfaces" Program (Award No. 152 37 00103).

REFERENCES

1. N.E. Penthorn, J.S. Schoenfield, J.D. Rooney and H. Jiang, "Reduction of charge impurities in a silicon metal-oxide-semiconductor quantum dot qubit device patterned with nano-imprint lithography." Nanotechnology 30, 465302 (2019).

2. L. Lin, J. Zhang, H. Su *et al.*, "Towards super-clean graphene." Nat. Commun. 10, 1912 (2019).

3. A. Rosenhahn, S. Schilp, H.J. Kreuzer and M. Grunze, "The role of inert surface chemistry in marine biofouling prevention." Phys. Chem. Chem. Phys. 12(17), 4275 (2010).

4. L. Zeng, N. Fady, S. Balachandar and P. Fischer, "Force on a finite-sized particle located close to a wall in a linear shear flow." Phys. Fluids 21(3), 033302 (2009).

5. P. Vasseur and R.G. Cox, "The lateral migration of a spherical particle in two-dimensional shear flows." J. Fluid Mech. 78, 385 (1976).

6. S.I. Rubinow and J.B. Keller, "The transverse force on a spinning sphere moving in a viscous fluid." J. Fluid Mech. 11, 447 (1961).

7. J. Schwarze, M. Grunze, M. Karahka and H.J. Kreuzer, “Attachment and detachment of particles from a surface under shear flow.” J. Phys. Chem. C 123, 8153–8159 (2019).

8. H. Lee, M.Y. Ha and S. Balachandar, “Rolling/sliding of a particle on a flat wall in a linear shear flow at finite Re.” Int. J. Multiphase Flow 37, 108–124 (2011).

9. H. Lee and S. Balachandar, “Drag and lift forces on a spherical particle moving on a wall in a shear flow at finite Re.” J. Fluid Mech. 657, 89–125 (2010).

10. A. Goldman, R.G. Cox and H. Brenner, “Slow viscous motion of a sphere parallel to a plane wall – I. Motion through a quiescent fluid.” Chem. Eng. Sci. 22, 637–651 (1967).

11. P.G. Saffman, “The lift on a small sphere in a slow shear flow.” J. Fluid Mech. 22, 385–400 (1965).

12. B. Andreotti and J.H. Snoeijer, “Statics and dynamics of soft wetting.” Annu. Rev. Fluid Mech. 52, 285–308 (2020).

13. J. Bico, E. Reyssat and B. Roman, “Elastocapillarity: when surface tension deforms elastic solids.” Anu. Rev. Fluid Mech. 50, 629–659 (2018).

14. J. Xie, J. Xu, W. Shang and K. Zhang, “Mode selection between sliding and rolling for droplet on inclined surface: effect of surface wettability.” Int. J. Heat Mass Transf. 122, 45–58 (2018).

15. R.W. Style, A. Jagota, C.-Y. Hui and E.R. Dufresne, “Elastocapillarity: surface tension deforms elastic solids.” Annu. Rev. Fluid Mech. 50, 629–659 (2018).

16. B. Andreotti, O. Baumchen, F. Boulogne, K.E. Daniel, E.R. Dufresne, H. Perrin, T. Salez, J.H. Snoeijer and R.W. Style, “Solid capillarity: when and how does surface tension deform soft solids?” Soft Matter 12, 2993–2996 (2016).

17. A.C. Balazs, T. Emrick and T.P. Russell, “Nanoparticle polymer composites: where two small worlds meet.” Science 314, 1107–1110 (2006).

18. Y. Yu, R.A. Lopez de al Cruz, B.D. Kieviet, H. Gojzewski, A. Pons, G.J. Vancso and S. de Beer, “Pick up move and release of nanoparticles utilizing co-non-solvency of PNIPAM brushes.” Nanoscale 9, 1670–1675 (2017).

19. L.I. Klushin, A.M. Skvortsov, A.A. Polotsky, S. Qi and P. Schmid, “Sharp and fast: sensors and switches based on polymer brushes with adsorption-active minority chains.” Phys. Rev. Lett. 113, 068303 (2014).

20. H. Merlitz, G.-L. He, C.-X. Wu and J.-U. Sommer, “Nanoscale brushes: how to build a smart surface coating.” Phys. Rev. Lett. 105, 115702 (2009).

21. X. Liu, Y. Li, J. Hu, J. Jiao and J. Li, “Smart moisture management and thermoregulation properties of stimuli-responsive cotton modified with polymer brushes.” RSC Adv. 4, 63691–63695 (2014).

22. W. Yang and F. Zhou, “Polymer brushes for antibiofouling and lubrication.” Biosurface and Biotribology 3, 97–114 (2017).

23. V.P. Nguyen, P.Q. Phi and S.T. Choi, “Tribological behavior of grafted nanoparticle on polymer-brushed walls: a dissipative particle dynamics study.” ACS Appl. Mater. Interfaces 11, 11988–11998 (2019).

24. J.A. Howarter and J.P. Youngblood, “Self-cleaning and anti-fog surfaces via stimuli-responsive polymer brushes.” Adv. Mater. 19, 3838–3843 (2007).

25. D. Bhandary, Z. Benková, M. Natália, D.S. Cordeiro and J.K. Singh, “Molecular dynamics study of wetting behavior of grafted thermo-responsive PNIPAAm brushes.” Soft Matter 12, 3093 (2016).

26. F. Léonforte and M. Müller, “Statics of polymer droplets on deformable surfaces.” J. Chem. Phys. 135, 214703 (2011).

27. L.I.S. Mensink, J.H. Snoeijer and S. de Beer, “Wetting of polymer brushes by polymeric nanodroplets.” Macromolecules 52, 2015–2020 (2019).

28. D. Daniel, A.Y.T. Chia, L.C.H. Moh, R. Liu, X.Q. Koh, X. Zhang and N. Tomczak, “Hydration lubrication of polyzwitterionic brushes leads to nearly friction- and adhesion-free droplet motion.” Commun. Phys. 2, 105 (2019).

29. P.R. Desai, Y. Wang, H.S. Sachar, H. Jing, S. Sinha and S. Das, “Supersolvophobic soft wetting: nanoscale elastocapillarity, adhesion, and retention of a drop behaving as a nanoparticle.” Matter 1, 1262–1273 (2019).

30. K. Speyer and C. Pastorino, “Droplet transport in a nanochannel coated by hydrophobic semiflexible polymer brushes: the effect of chain stiffness.” Langmuir 33, 10753–10763 (2017).

31. S. Biagi, L. Rovigatti, F. Sciortino and C. Misbah, “Surface wave excitations and backflow effect over dense polymer brushes.” Sci. Rep. 6, 22257 (2016).

32. X.Z. Jiang, M. Feng, Y. Ventikos and K.H. Luo, “Regimes of flow over complex structures of endothelial glycocalyx: a molecular dynamics simulation study.” Sci. Rep. 8, 5732 (2018).

33. L. Lanotte, G. Tomaiuolo, C. Misbah, L. Bureau and S. Guido, “Red blood cell dynamics in polymer brush-coated microcapillaries: a model of endothelial glycocalyx *in vitro*. Biomicrofluidics 8, 014104 (2014).

34. J. Fan, M.C.T. Wilson and N. Kapur, “Displacement of liquid droplets on a surface by a shearing air flow.” J. Colloid. Interf. Sci. 356, 286–292 (2011).

35. L. Mahadevan and Y. Pomeau, “Rolling droplets.” Phys. Fluids 11(9), 2449–2453 (1999).

36. S. Basu, K. Nandakumar and J.H. Masliyah, “A model for detachment of a partially wetting drop from a solid surface by shear flow.” J. Colloid Interf. Sci. 190, 253–257 (1997).

37. E. Ezzatneshan and R. Goharimehr, “Study of spontaneous mobility and imbibition of a liquid droplet in contact with fibrous porous media considering wettability effects.” Phys. Fluids 32, 113303 (2020).

38. M. Kumar, R. Bhardwaj, K.C. Sahu, “Motion of a droplet on an anisotropic micro-grooved Surface.” Langmuir 35(8), 2957–2965 (2019).

39. S.-G. Kim and W. Kim. "Drop impact on a fiber." Phys. Fluids 28(4), 042001 (2016).

40. P.J. Hoogerbrugge and J.M.V.A. Koelman, “Simulating microscopic hydrodynamic phenomena with dissipative particle dynamics.” Europhys. Lett. 19, 155–160 (1992).

41. R.D. Groot and P.B. Warren, “Dissipative particle dynamics. Bridging the gap between atomistic and mesoscopic simulation.” J. Chem. Phys. 107, 4423–4435 (1997).

42. P. Español and P. Warren, “Statistical mechanics of dissipative particle dynamics.” Europhys. Lett. 30, 191–196 (1995).

43. P. Malfreyt and D.J. Tildesley, “Dissipative particle dynamics simulations of grafted polymer chains between two walls.” Langmuir 16, 4732–4740 (2000).

44. D. Irfachsyad, D.J. Tildesley and P. Malfreyt, “Dissipative particle dynamics simulation of grafted polymer brush under shear.” Phys. Chem. Chem. Phys. 4, 3008–3015 (2002).

45. F. Goujon, P. Malfreyt and D.J. Tildesley, “Mesocopic simulation of entanglements using dissipative particle dynamics: application to polymer brushes.” J. Chem. Phys. 129, 034902 (2008).

46. G.S. Grest and K. Kremer, “Molecular dynamics simulation for polymers in the presence of a heat bath.” Phys. Rev. A 33, 3628–3631 (1986).

47. D. Pan, N. Phan-Thien and B.C. Khoo, “Studies on liquid-liquid interfacial tension with standard dissipative particle dynamics method.” Mol. Simul. 41(14), 1166–1176 (2015).

48. M.A. Seaton, R.L. Anderson, S. Metz and W. Smith, “DL MESO: Highly scalable mesoscale simulations.” Mol. Simul. 39, 796 (2013).

49. D.I. Dimitrov, A. Michev and K. Binder, “Polymer brushes in solvents of variable quality: molecular dynamics simulations using explicit solvent.” J. Chem. Phys. 12, 084905 (2007).

50. A. Marchand, D. Siddhartha, J.H. Snoeijer and B. Andreotti, “Contact angles on a soft solid: from Young’s Law to Neumann’s Law.” Phys. Rev. Lett. 109, 236101 (2012).

51. Z. Cao and A.V. Dobrynin, “Polymeric droplets on soft surfaces: from Neumann’s triangle to Young’s law.” Macromolecules 48, 443–451 (2015).

52. M.A. Hubbe, “Theory of detachment of colloidal particles from flat surfaces exposed to flow.” Colloids Surf. 12, 151–178 (1984).

53. S. Ramanujan and C. Pozrikidis, “Deformation of liquid capsules enclosed by elastic membranes in simple shear flow: large deformations and the effect of fluid viscosities.” J. Fluid Mech. 361, 117–143 (1998).

54. I. Cantat and C. Misbah, “Lift force and dynamical unbinding of adhering vesicles under shear flow.” Phys. Rev. Lett. 83(4), 880–883 (1999).

55. J. Beaucourt, T. Biben and C. Misbah, “Optimal lift force on vesicles near a compressible substrate.” Europhys. Lett. 67(4), 676–682 (2004).

56. H.S. Davies, D. Débarre, N.E. Amri, C. Verdier, R.P. Richter and L. Bureau, “Elastohydrodynamic lift at a soft wall.” Phys. Rev. Lett. 120, 198001 (2018).

57. J.M. Skotheim and L. Mahadevan, “Soft lubrication.” Phys. Rev. Lett. 92(24), 245509 (2004).